

Nanosecond Laser-Driven Semiconductor Switch for 70 GHz Microwave Radiation

Maxim Kulygin · Gregory Denisov

Received: 21 November 2011 / Accepted: 13 April 2012 /
Published online: 4 May 2012
© Springer Science+Business Media, LLC 2012

Abstract We study a new type of semiconductor switches for microwave radiation driven by laser emission. The switches comprise a plate of plain semiconductor built in a hollow metallic waveguide resonator. The plate can be illuminated by laser emission changing the resonator properties due to photoconductivity and therefore switching between two stable states. A sample switch has been built and experimentally investigated, demonstrating nanosecond level of switching performance. The results of numerical simulation by the FDTD method are compared with the experimental data. Typical laser pulse energies sufficient for switching are from 1 nJ to 100 nJ, switched radiation frequency tuning range is about 10 % around 70 GHz. The switching operation was observed in wide range of the driving 100-femtosecond laser parameters - for pulse energy from 6 pJ to 250 μ J, and laser emission wavelength from 0.75 μ m to 2 μ m.

Keywords Microwave devices · Photoconducting devices · Semiconductor switches · FDTD · Waveguides

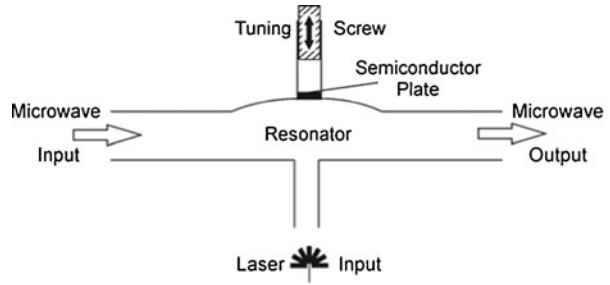
1 Introduction

Laser driven switches for microwave radiation are based on an induced photoconductivity effect in semiconductor elements changing properties of resonant systems they are built in [1, 2]. The switches are used for commutation of powerful microwave radiation beams in plasma heating, particle accelerators, radars, *etc.* The prospective applications often require switching rapidness up to nanoseconds, tolerance to commutated power up to kilo- and megawatts, commutated radiation frequencies up to hundreds of gigahertz or terahertz, and coherence of output pulse packets between each other. The switches studied in this work could be one of the most promising to satisfy these requirements.

Figure 1 represents a layout of the 70 GHz semiconductor switch with one-side copper waveguide widening resonator. It is surrounded with two symmetrical pieces of standard

M. Kulygin (✉) · G. Denisov
Institute of Applied Physics (IAP), RAS, Nizhny Novgorod, Russia
e-mail: kmaxim@appl.sci-nnov.ru

Fig. 1 Layout of the semiconductor switch for 70 GHz microwave radiation.



3.6 mm × 1.8 mm single TE₁₀ eigenmode rectangular waveguide for the input and the output of the commutated microwave radiation. The resonator also has two attached pieces of subcritical waveguide for eigenmode coupling. The lower waveguide is also used as the input for laser emission.

The semiconductor plate is located at the junction of the resonator and the upper waveguide. The working principle of the resonator is similar to a notch filter [3] which suppresses the passing microwave with a selected frequency to the level of about -40 dB. The screw located above the plate is used for mechanical tuning of the frequency. Illuminating the plate by an appropriate laser emission significantly changes the resonator frequency and its quality factor so the previously reflected signal can pass through it unchanged. This is the switching.

2 Theory and numerical simulation

In this study all calculations are based on the simplified theory of switches [4]. We have a set of Maxwell’s equations for the fields *E* and *H* in vacuum and semiconductor media:

$$\text{rot}\vec{E} = -\frac{1}{c} \frac{\partial\vec{H}}{\partial t}, \tag{1}$$

$$\text{rot}\vec{H} = \frac{1}{c} \left(\varepsilon \frac{\partial\vec{E}}{\partial t} + 4\pi eN(\vec{r}, t)\mu\vec{E} \right). \tag{2}$$

Here *c* is a light velocity, ε is a permittivity, *e* is an electron charge, and μ is total charge carrier mobility for the semiconductor. *N* is total charge carrier density (electrons and holes) in the semiconductor, also time dependent:

$$\frac{\partial N}{\partial t} = D\Delta N + g(\vec{r}, t) - G_1(N - N_e). \tag{3}$$

Here *D* is an ambipolar diffusion coefficient, *g*(*r*; *t*) is a source of photoconductivity [4], *G*₁ is a charge carrier recombination constant obtained from auxiliary measurements of the semiconductor sample, and *N*_{*e*} is a typical equilibrium density for room temperature. Further details of the theory and the boundary conditions have been published before in [4]. Similar theoretical principles can be found in the early work of [5]. All typical semiconductor constants can be found in [6].

For numerical simulations of the system (1)–(3) we use an own software based on a modification [7] of the well-known Finite Difference Time Domain (FDTD) method [8]. This also includes Unsplit Perfectly Matched Layer (UPML) absorbing boundary conditions [9] at all the ends of waveguides, Ohmic loss boundary conditions at the positions of copper walls, and a transparent unidirectional TE_{10} wave source near the input.

We supposed our numerical model to make adequate calculations at the microwave frequency band between 50 and 100 GHz. So the spatial grid step is $25\ \mu\text{m}$, and $0.1\ \mu\text{m}$ in the photoconductivity layer due to big difference of charge carrier density. The basic time step is 117 fs; it corresponds to a Courant number [8] value of 0.99. The time step is automatically adjusted by the software to keep the Eq. (3) stable all over the time of simulation:

$$dN(\vec{r}, t) \ll N(\vec{r}, t), \quad (4)$$

where dN means an increment to the density at each time step.

The simulation software consumes about 10 Mbytes of memory. On a modern personal computer the calculation performs at about 0.5 ns per a processor core per a minute of real time. The total times of simulation did not exceed 100 ns.

3 Frequency characteristics

Frequency characteristics of the switch are calculated by the FDTD method as an output response to an input microwave signal with wide spectrum. So we can find all resonances and optimize the geometry of the switch to have a single resonance without overlapping in the frequency range of interest. Once the resonance is found we can obtain field structure for the switch with quasi-monochromatic microwave signal on its input at the resonant frequency. Figure 2 shows electric field plots for an optimized geometry and quasi-monochromatic microwave signal at the frequency of 70 GHz. Black color means zero field amplitude, white means maximum.

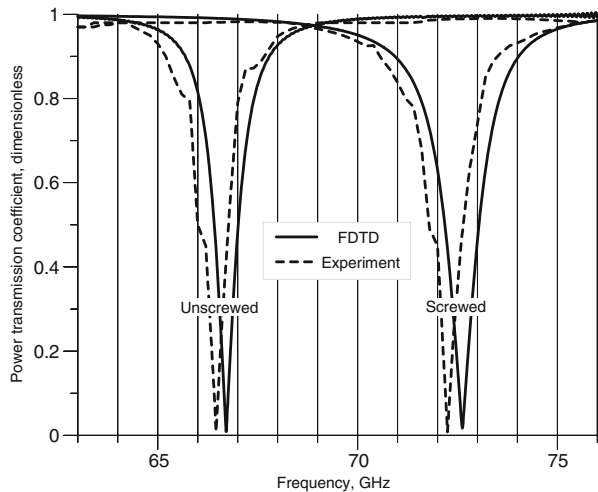
The switch is closed at this frequency when the laser is off (the microwave is in resonance and it is mostly reflected from the switch) and open when the laser is on (the resonance is broken and the wave passes through without reflection).

The resonant frequency of the switch can be mechanically fine-tuned with the tuning screw located at the upper subcritical waveguide. The frequency increases as the screw approaches the semiconductor plate. Power-frequency characteristics of the geometry-optimized switch without laser are shown at Fig. 3 for “unscrewed” and tightly “screwed” cases. FDTD calculation results are displayed by the solid lines and the corresponding experimental data are displayed by the dashed lines. The difference between the theory and the experiment is about 1 %; this is due to the switch’s fabrication imprecision and measurement errors.



Fig. 2 Electric field plots for 70 GHz microwave; left—laser off and the switch closed, right—laser on and the switch open.

Fig. 3 Power-frequency curves of the switch—theory vice experiment.



We can see that the frequency of the switch can be shifted for about 10 % from about 66.5 GHz, when the screw is totally removed (see Fig. 1), to about 72.5 GHz, when the distance between the plate and the edge of the screw is minimal—about 0.3 mm. The frequency can be shifted higher but it causes degradation of the resonance. Also the minimal distance is limited for the plate's safety.

4 The semiconductor plate

We use gallium arsenide (GaAs) for this semiconductor switch due to its nanosecond level of photoconductivity relaxation [6]. The exact value of the relaxation constant G_I from (3) is obtained from measurements of luminescence relaxation in GaAs samples, it ranges from 10^9 to 10^{10} s^{-1} .

The thickness of the plate is a subject to optimization. It is obvious that plates thinner than 50 μm cannot effectively reflect 70 GHz electromagnetic waves even when illuminated by a laser. In addition such plates are extremely fragile. At the same time plates thicker than 500 μm significantly reflect the electromagnetic waves even without a laser due to high permittivity of the semiconductor $\varepsilon_{\text{GaAs}}=12.96$. Also the optimal plate thickness should provide a resonance deep enough to make difference between open and closed states of the switch.

A typical depth of the resonance for the switch is about -40 dB and it's almost constant during the mechanical tuning by the screw. To prevent degradations adjacent resonances should not be overlapped by each other, this is reached by geometry optimization. Figure 4 shows a bar chart of resonances vice plate thickness and frequency. We can see that the optimum plate thickness ranges from 100 to 200 μm for frequencies about 70 GHz.

5 Experimental setup and frequency tuning

A working sample of the switch is displayed at Fig. 5. The longest dimension does not exceed 3 cm. The microwave input 3.6 mm \times 1.8 mm waveguide with connection pins and

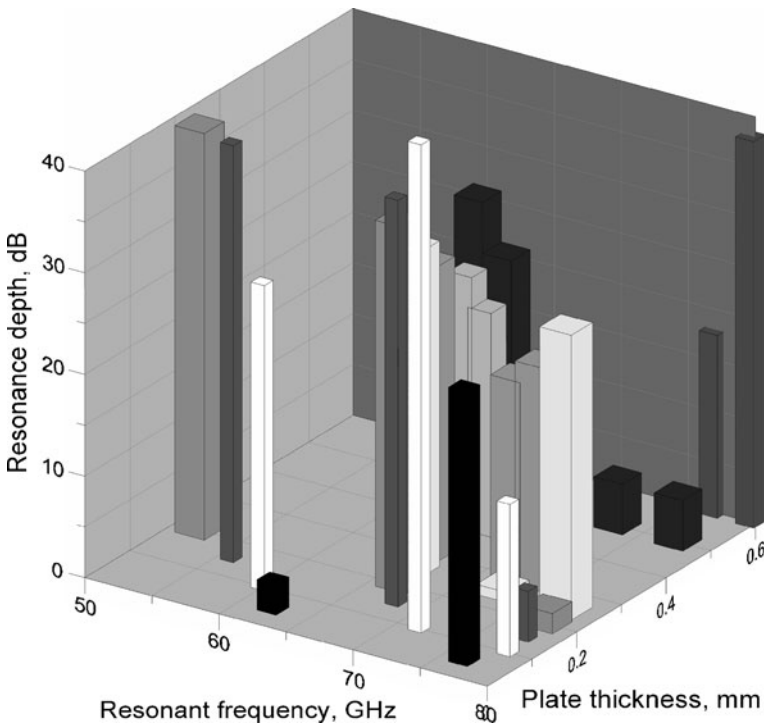


Fig. 4 Optimization of the GaAs plate thickness by depth and frequency.

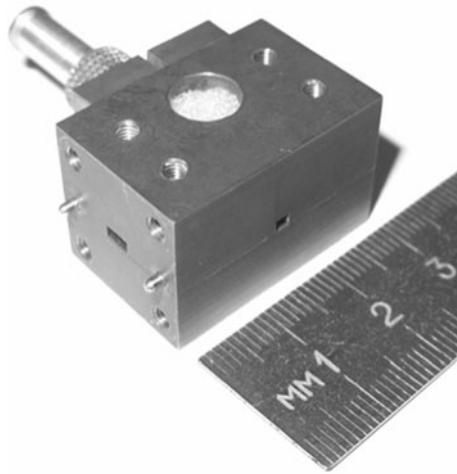
screw holes can be seen at the left side; it is symmetrical to the output. The lower side has the input for laser emission. The semiconductor plate is installed through the hole at the center. The frequency tuning screw with its flange is located on the higher side.

We have performed several experiments with the switch; the layout of the most complete experimental setup is shown in Fig. 6. The TE_{10} microwave from a frequency tunable source with power less than 1 W is fed to the input of the switch through a directional coupler to suppress the reflected signal. The pulse laser emission beam is focused at the semiconductor plate. The output is connected to a detector that transforms microwave energy to an electric voltage. The output of the detector is loaded with a 50Ω resistor to achieve a nanosecond level of performance. Then the detected output signal is directed to an oscilloscope. The digital oscilloscope has a frequency bandwidth of 500 MHz and a sampling rate of 5×10^6 samples per second.

6 Pulsed laser experiments

For this study we use a femtosecond titan-sapphire (Ti:Sa) laser complex consisting of a main Ti:Sa optical laser with diode pumping, a Ti:Sa optical regenerative amplifier and a parametric infrared amplifier. The main laser has pulse duration of 50–100 fs, wavelength of 750–830 nm, pulse repetition rate of 75.4 MHz, and average power of 500 mW (the pulse energy is about 10 nJ). The regenerative amplifier decreases the repetition rate to 1 kHz but increases the average power to 2.5 W (the pulse energy to 2.5 mJ). The parametric amplifier

Fig. 5 Photo of a working sample of the nanosecond switch for 70 GHz.



increases laser emission wavelength up to 2 μm providing an ability to observe a red boundary of photo effect and its influence on switching. The laser emission is guided to the switch through its 2 mm input; see Figs. 1, 5, 6.

A typical response of the switch to repetitive main laser pulses is series of the switched microwave pulse packets. Figure 7 displays it as an oscillogram curve of the detected signal amplitude. We can see the same repetition rate to the laser of 13.6 ns. The rise time of the microwave pulses is about 1 ns, the fall time is about 2 ns.

The main laser pulses have 100 fs duration that is negligible to the nanosecond time scale of the response; they correspond to the rise beginning of the detected pulses. The results are in good agreement with the FDTD simulation.

Figure 7 displays results for 10 nJ pulses of the main laser at 780 nm, the unity of the dimensionless amplitude corresponds to 35 mV at the oscilloscope. It is followed with an obvious experiment of investigating the detected voltage amplitude dependence on laser pulse energy; this is like a volt-ampere characteristic of integrated circuit devices. We use the main laser with the regenerative amplifier (it has 1 kHz output rate) at and attenuation filters to cover the whole scale of pulse energies. The obtained dependence is shown at Fig. 8

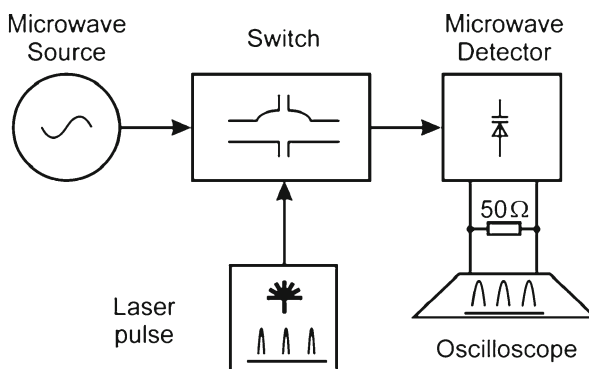
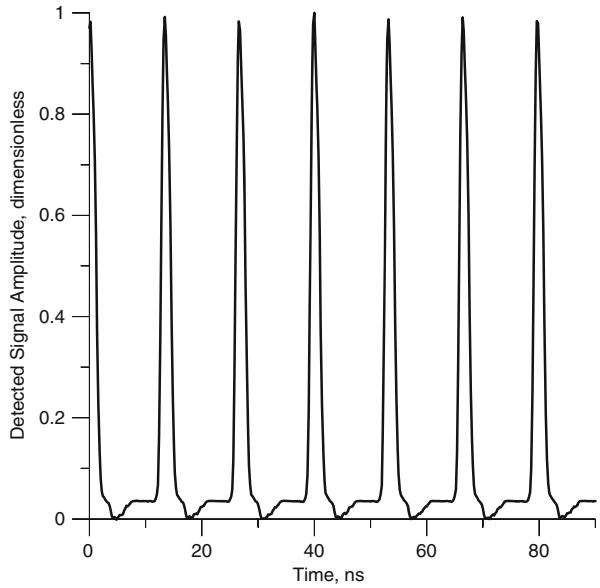


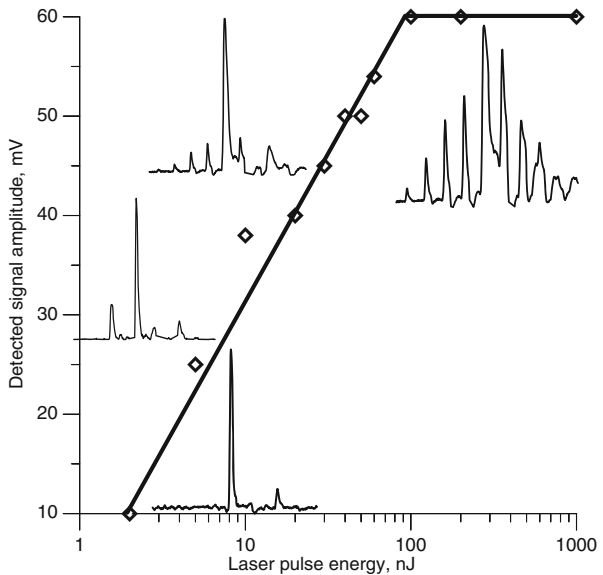
Fig. 6 Layout of the experimental setup.

Fig. 7 Detected output signal as a response to series of laser pulses.



where the square symbols correspond to measurement data. The approximation curve has a linear growth area in the range between 1 and 100 nJ, and a saturation with 60 mV constant response amplitude for higher energies. So the threshold level of saturation for the switch is 100 nJ. Several schematic response oscillograms in nanosecond time scale are also displayed at Fig. 8, they correspond to different laser pulse energy values. We can see the main response pulse widening as the pulse energy grows. Also we can see adjacent unamplified 75.4 MHz main laser pulses with comparable amplitudes, i.e. satellites; that shows a

Fig. 8 Detected signal amplitude vice laser pulse energy and respective detected signal oscillograms (schematically).



nonlinearity of the switch response. The nonlinearity of the switch itself combines several effects - saturation of the transmission coefficient on the laser power when it is close to 1, changes of the photoconductivity relaxation mechanism when the charge carrier density is higher than 10^{16} cm^{-3} , and internal nonlinearity of the microwave detector which is attached to the output of the switch. And these nonlinearities are overlaid by the regenerative amplifier nonlinearities at higher pulse energies, so that is the cause for the satellites before and after the main peak.

7 Red boundary of photo effect

Pure gallium arsenide has a red boundary of photo effect at the illuminating emission wavelength of 870 nm [6]. It means that we should observe no switching for the laser emission wavelength above this level. So we use the parametric laser amplifier that yields wavelengths from 750 nm to 2 μm . Figure 9 shows a bar chart of detected signal amplitude dependence on the laser wavelength and pulse energy.

Zero detector responses have been observed for 10 nJ pulses at 0.99 μm and for 20 nJ pulses at 1.06 μm . But we can see that the red boundary is not always a strict limit of functionality for the switch.

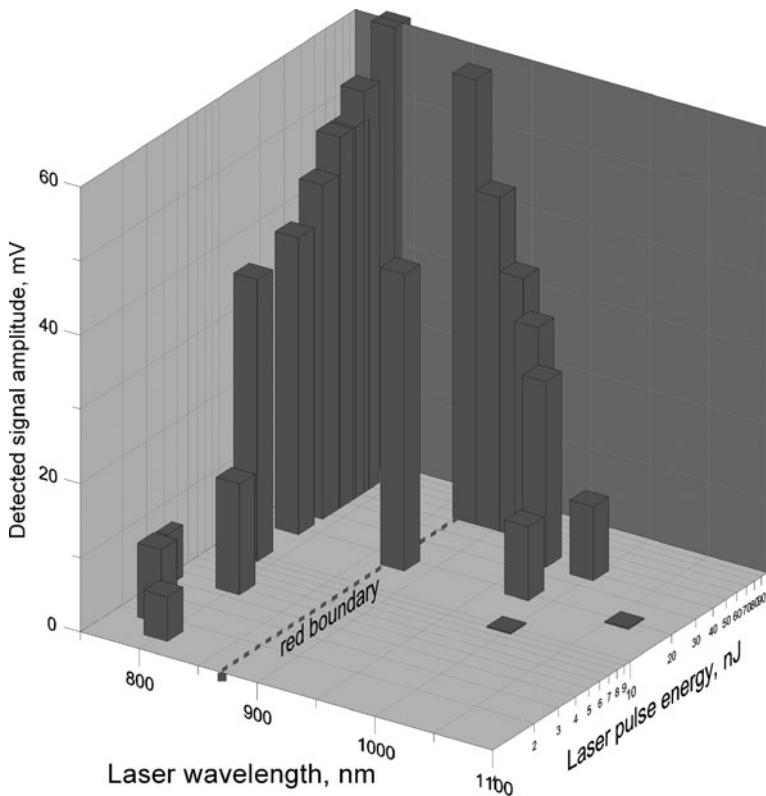


Fig. 9 The switch’s response to laser pulses around the red boundary.

Response degradation on crossing the red boundary is observed instead. For 2 μm laser wavelength we have also made response measurements, 25 nJ pulse caused zero response, 250 nJ pulse caused 10 mV response, and 25 μJ pulse caused a response with the maximum amplitude. So the maximum detected amplitude has been observed at all wavelengths in range from 0.75 μm to 2 μm but to keep the response constant the laser pulse energy has to be increased by 3 orders. The possible reasons of nonzero response beyond the red boundary of photo effect are wide spectrum of femtosecond laser pulses, impurities in used sample of gallium arsenide, and multi-photon photo effect.

8 Characteristic laser pulse energies

The fabricated sample of the switch has been found operational for a wide range of driving laser pulse energies and wavelengths. The target of the next experiment is to find lower pulse energy when the detected switch response vanishes in noise. We use the main laser with wavelength of 806 ± 7 nm, repetition rate of 75.4 MHz and pulse duration of 100 fs. The maximum pulse energy is 10 nJ in this experiment; it is consequently reduced and the detector response amplitude is measured. The digital oscilloscope loses fidelity for voltages lower than 10 mV, so we have additionally used a lock-in amplifier that is able to register 75.4 MHz pulses with amplitude down to 1 nV. The results are displayed at Fig. 10.

The dashed curve is the amplitude measured by the oscilloscope; it starts to vanish in digital noise at about 5 mV. The solid curve is the RMS voltage measured by the lock-in amplifier that is lower than the oscilloscope data. There is no change at 3 μV and energy lower than 6 pJ. So this is the lower energy limit for the switch.

Testing the switch at much higher laser pulse energy we have found another characteristic energy level of about 1 μJ . Above this level the detected signal voltage did not come back to zero after completion of the main pulse and its satellites from the regenerative amplifier laser. A typical oscillogram curve is shown at Fig. 11.

Fig. 10 Detected signal voltage vice laser pulse energy.

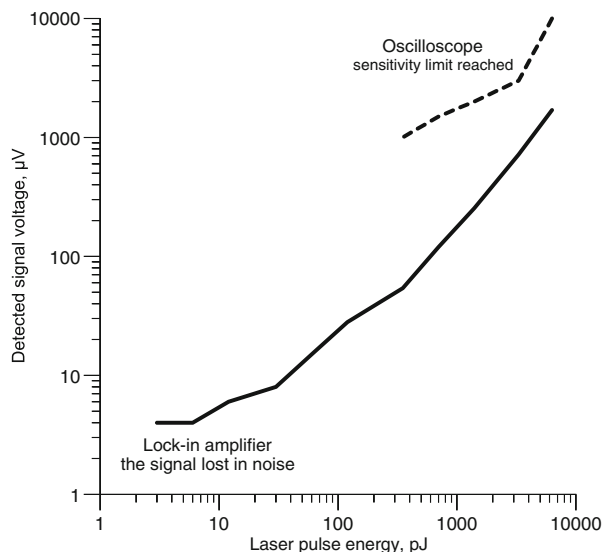
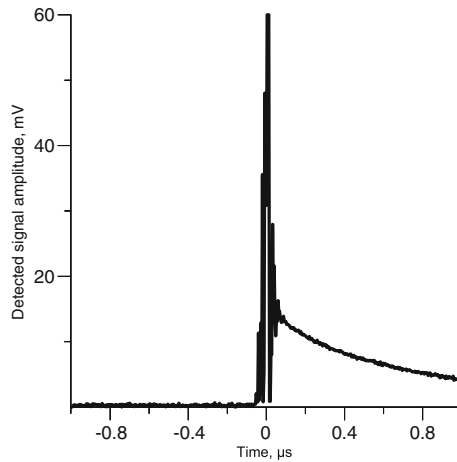


Fig. 11 Detected output signal at laser pulse energy of $6 \mu\text{J}$.

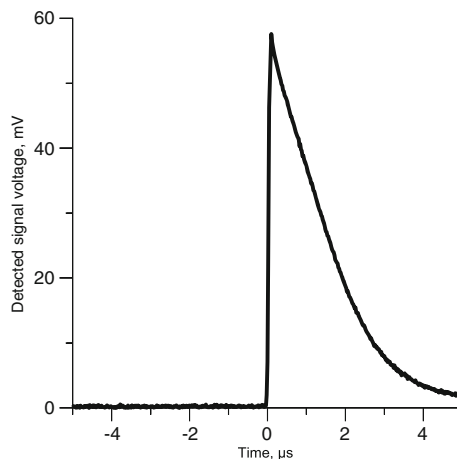


The complete relaxation of detected signal is observed after several microseconds from the laser pulse. Figure 12 displays a case of $250 \mu\text{J}$, the maximum laser pulse energy we have used for experiments. Higher energies obviously put the semiconductor plate at risk of permanent damage. The most likely reason of this microsecond scale process is thermal relaxation of the semiconductor.

9 Conclusion

The switch demonstrates nanosecond level of performance. It provides a broad frequency tuning range of about 10 % so it has low requirements for fabrication precision. It remains operational in wide range of driving laser parameters so there is a possibility of using inexpensive modern $1.06 \mu\text{m}$ infrared lasers instead of bulky optical multi-cascade sets. The switch seems to be especially useful for molecular coherent spectroscopy. Attached to a source of coherent microwaves it can modulate the monochromatic source to series of

Fig. 12 Detected output signal at laser pulse energy of $250 \mu\text{J}$.



packets with nanosecond duration. And all the packets at the output of the switch have phases linked to each other. So there is a possibility to expand the spectrum of molecular analysis and improve its resolution.

Although we tested the switch at commutated microwave power less than 1 W we expect the switch to withstand much higher power.

Acknowledgment The authors thank Yu. V. Rodin, B. V. Shishkin and I. E. Ilyakov for their assistance in experiments, V. V. Korchagin and E. A. Novikov for the switch fabrication, and V. Ya. Aleshkin for useful discussions.

References

1. T. Fumihiko and S. G. Tantawi, “Development of high power X-band semi-conductor microwave switch for pulse compression systems of future linear colliders,” *Phys. Review special topic—Accelerators and beams*, vol.5, 062001, 2002.
2. A. A. Vikharev, G. G. Denisov, Vl. V. Kocharovskiy, S. V. Kuzikov, V. V. Parshin, N. Yu. Peskov *et al.*, “A high-speed quasi-optical wave phase switch based on the induced photoconductivity effect in silicon,” *Tech. Phys. Lett.*, 2007, vol. 33, No. 9, pp. 735–737.
3. G. G. Denisov, S. V. Kuzikov and D. A. Lukovnikov, “Simple millimeter wave notch filters based on rectangular waveguide extensions,” *Int. J. of IRMM Waves*, 1995, vol. 16, No. 7, p. 1231.
4. M. L. Kulygin, G. G. Denisov, Vl. V. Kocharovskiy, “Modeling of dynamic effects in a laser-driven semiconductor switch of high-power microwaves,” *Int. J. of IRMM and THz waves (IJIM)*, Springer, 2010, vol. 31, issue 1, pp. 31–40.
5. L. I. Katz, A. A. Safonov, “Interaction of electromagnetic microwaves with semiconductor charge carrier plasma,” Saratov University press, USSR, 1979.
6. O. Madelung, *Semiconductors, Data Handbook*. Springer, 2003.
7. M. L. Kulygin (2006 Jun 19), *Numerical investigation of three-dimensional multi-mode electrodynamic systems of electronic microwave devices*, Ph.D. report monograph. IAP RAS, Nizhny Novgorod, Russia, pp. 12–47.
8. A. Taflove, *Computational electrodynamics: the finite-difference time-domain method*, Boston, MA: Artech House, 1995.
9. S. D. Gedney, “An anisotropic perfectly matched layer—absorbing medium for the truncation of FDTD lattices”, *IEEE Trans. Antennas and Propagation*, 1996, vol. 44, No. 12, p. 1630.